

Scalar superradiance in the charged black-bounce spacetimes

Zhiming Shuai,^{1,*} Xiangdong Zhang,^{1,†} and Gui-Rong Liang^{2,‡}

¹*School of Physics and Optoelectronics, South China University of Technology, Guangzhou 510641, China*

²*School of Materials Science and Physics, China University of Mining and Technology, Xuzhou 221116, China*

We numerically investigate the superradiant amplification effect of a charged scalar field in the scattering experiment and the black hole bomb model in a charged black-bounce spacetime. Due to the shallowing effect on the effective potential by the introduced quantum parameter λ , superradiance in both the above cases are verified to be weakened. In a scattering experiment, the quantum parameter and the field mass suppress the amplification in all frequency ranges, while the black hole and field charge influence it differently in high and low frequencies. In a Type I black hole bomb model, where the reflective mirror is placed outside the ergo-region, we find a new distinct eigen-mode for the scalar field evolution in a high λ value, which is however absent in the case of Type II black bomb where the mirror is set inside the ergo-region. Moreover, we investigate the heavy field mass scenario in a Type II black hole bomb and find no amplification effect in this confined configuration.

arXiv:2511.04007v1 [gr-qc] 6 Nov 2025

* 202410188403@mail.scut.edu.cn

† Corresponding author: scxdzhang@scut.edu.cn

‡ Corresponding author: bluelgr@sina.com

I. INTRODUCTION

The phenomenon of superradiance exhibits wave amplification of fields in a thermodynamic system, with the cost of dissipation in a “viscous medium”. The first example was given by the so called “Klein paradox” [1, 2], in which charged bosons get energy enhancement when scattered by a potential barrier where particle-antiparticle pair creations are excited [3]; the antiparticles with negative energy were injected into the barrier and particles with positive energy joint into the original particle beam and reflected. Energy conservation is kept and necessary during the process. Fermions does not possess such amplification due to the positive definiteness of its energy current density, in the quantum field point of view, it is Pauli exclusion principle that limits numbers of pair productions [4] to form a macroscopic negative current. In curved spacetime, superradiance can also occur in vacuum [3]; especially in black hole (BH) physics, the existence of the event horizon render the BH behave as a “viscous one-way membrane”, such that an intrinsic dissipative region is provided in the form of an ergoregion, where timelike particles can have negative energies with respect to infinite observers. In Penrose thought experiment [5], particle splitting take place in a similar manner, however in a classical sense, with that of pair creation in Klein paradox, such that energy of BHs is extracted, which happens both in rotation and charged static background. The wave analogue comes parallel in the low-frequency regime, followed by quantitative analysis in pioneering works in Kerr [6, 7] and Reissner-Nordström (RN) [8] spacetimes. The ergoregion is intrinsic in rotating case, but an effective description in charged static case where it includes both information of the curvature and properties of the field, e.g., mass and charge, and may even cover the whole exterior of the black hole [9].

Superradiant instabilities occur in the sense that the process can be carried repeatedly, when a reflective mechanism is provided in a distant region to bounce the amplified wave back again. In the rotation case, the mass of the bosonic field itself serves as a natural mirror to bound the condensing cloud, while asymptotically-flat charged BHs were shown to be stable against massive charged scalar perturbations [10, 11], hence a reflective boundary must be imposed in a toy model, to make a so-called “black hole bomb” [12]. In contrast to the astronomical relevance in the rotating case [13–24], the increasing investigations on superradiance in charged static system [25–33] makes it more interesting from a conceptual point of view: Its remarkably short instability time scale makes it an ideal testbed for fully nonlinear studies of black hole instabilities within cavities, in [34, 35], the researchers employ an asymptotically flat, spherically symmetric spacetime with a boundary at a fixed coordinate distance

where the charged scalar field adheres to Dirichlet conditions. This framework permits tracking the linearized instability into the nonlinear regime, with substantial evidence indicating a final entropically preferred state where a black hole is surrounded by a charged condensate [36]. Moreover, the occurrence of superradiance in static charged black holes plays a vital role in enabling diverse applications within the gauge/gravity duality framework. Notable examples include the mechanism of spontaneous symmetry breaking in the vicinity of a Reissner-Nordström anti-de Sitter (RN-AdS) black hole [37], as well as associated developments in holographic superconductor models [38]. Research on charged black hole bombs has progressed through both analytical treatment [39, 40], and numerical approaches in which the behaviors were examined at the linear field amplitude level in both frequency and time-domain [41–43]. Generalizations were carried for a charged massless scalar field in the spacetime of a charged stringy black hole with mirror-like boundary conditions [44, 45], and in the context of massive charged scalar fields on a Kerr-Newman background [46], which confirms even in the rotation-dominated regime the instability growth rate depends on the coupling between the field charge and the black hole charge.

On the other hand, it is widely believed that quantum gravity effects would remove the curvature singularity of a black hole and result a regular/non-singular black hole [47]. However, since a complete theory of quantum gravity is not yet well established, investigations on various non-singular black holes at the phenomenological level were extensively carried. Although these models are usually not any solutions to the vacuum Einstein equation, one can fix the logic by introducing some exotic matter field on the right hand side of the equation. Regular black holes can be traced back to the well known Bardeen black hole [48], Hayward black hole [49] as well as other notable regular black hole models [50–53]. The properties of regular black holes were studied with the purpose of revealing the internal structure of black holes and capturing the signals due to the possible quantum gravity effect. In recent years, investigations on the superradiant effect and black hole bomb instability of different types of regular black holes were carried increasingly [54–59], which provided interesting insights in understanding the interplay between fundamental and phenomenological aspects.

In this paper, we investigate the superradiant effects in a spherically symmetric charged black-bounce spacetime [60, 61], which allows a special class of regular black holes and wormhole solutions in a smooth parameter tuning. The metric could be achieved by a radial coordinate transformation $r \rightarrow \sqrt{r^2 + \lambda^2}$, with λ a length scale parameter representing quantum regularization, to deform the classical Reissner-Nordström (RN) metric to the black-bounce-RN geometry [62–66]. The introduced parameter is typically associated with the Planck length, which smooths the central singularity while

preserving asymptotic RN behavior. The model provides a phenomenological framework to probe how quantum gravitational effects alter the dynamics of superradiant processes and black hole bombs, and allows us for a controlled comparison with classical results by tuning λ . The primary focus of this work is to analyze how this length scale parameter influence two interconnected phenomena, the efficiency of superradiant energy extraction from the black hole, and the instabilities of black hole bomb.

The remainder of the paper is organized as follows. In section II, we will briefly review basic properties of the black-bounce-RN spacetime, as well as the dynamics of a charged scalar field propagating on this background. By the Regge-Wheeler analysis, we extract the effective potential, and investigate how it is influenced by different choices of the quantum parameter. Through physical inspections, we predict the tendency how the parameter λ would affect the superradiant amplification, which is to be verified and confirmed in following contexts. Then we numerically explore the influence of each parameter in the metric on the amplification factor in a scattering experiment, and observe the dependence in each frequency band. In section III, we numerically study the superradiant amplification of the scalar field in two types of black hole bomb models, where the reflective mirror described by a Dirichlet boundary condition is put outside or inside the ergo-region. To mimic the purely ingoing boundary condition, the perfectly matched layer (PML) [67–69] method is employed and tested. In solving the differential equation in the time domain, the finite difference method combined with the method of lines are used, and the eigenvalues are extracted from the wave amplitude evolution by a discrete Fourier transform. To gain the energy flux, we invoke a type of constructed conserved energy current out of the energy-momentum tensor. In a Type II black bomb model, we further investigate the heavy field mass scenario where the field is in a confined configuration. Results are shown mainly in the form of diagrams, and we exhibit findings in the adjoint contexts. In section IV, we conclude and re-organize the logic presented in the main contexts, and outlook some possible extentions. Throughout the paper, we adopt the $(-, +, +, +)$ signature in the metric and the natural units $c = G = \hbar = 1$.

II. DYNAMICS OF CHARGED SCALAR FIELDS IN BLACK-BOUNCE-REISSNER-NORDSTRÖM SPACETIMES

In this section, we will briefly review the black-bounce-Reissner-Nordström spacetimes [60], inspired by the uncharged black-bounce spacetime [62], which is a type of black hole without singularity. Performing the regularizing replacement $r \rightarrow \sqrt{r^2 + \lambda^2}$ in the RN metric, with λ a length scale parameter typically associated with the Planck length, we obtain the following line element

$$\begin{cases} ds^2 = -f(r) dt^2 + f(r)^{-1} dr^2 + (r^2 + \lambda^2) d\Omega^2, \\ f(r) = 1 - \frac{2M}{\sqrt{r^2 + \lambda^2}} + \frac{Q^2}{r^2 + \lambda^2}, \end{cases} \quad (1)$$

with M and Q the BH mass and electric charge. Note that the replacement extends the natural domain of the radial coordinate r from $[0, +\infty]$ to $[-\infty, +\infty]$, and asymptotic flatness is preserved. It is verified by calculating the Kretschmann scalar and curvatures, this replacement smooths the geometry globally regular, rather than simply making a coordinate transformation [60]. The metric is controlled precisely in a minimal manner to describe regular BHs and traversable wormholes smoothly, as we can check that when $M \rightarrow 0$ and $Q \rightarrow 0$ it recovers the standard Morris-Thorne wormhole [60, 70–72]. The horizons can be obtained by $f(r) = 0$ which gives

$$r_{\pm} = \sqrt{\left(M \pm \sqrt{M^2 - Q^2}\right)^2 - \lambda^2}, \quad (2)$$

where the existence of horizons is guaranteed by a range of parameter choices satisfying $|Q| < M$ and $|\lambda| < M + \sqrt{M^2 - Q^2}$.

Though the propose of the metric is due to quantum gravity effects, we can also understand it in a way that the metric is described by general relativity, with the determination of the associated non-trivial matter/energy content is determined the Einstein equation, with which we could fix the geometro-dynamics. It is verified that outside the outer horizon, the radial null energy condition (NEC) is violated, hence the weak, strong and dominant energy conditions all violated [62]. With the help of Einstein equation, non-zero components of the the energy-momentum tensor can be computed. The explicit form of the tensor can be decomposed into two parts, in which one is the usual Maxwell stress-energy tensor, and the other is interpreted as the “charged dust” [60], with its density involving both the bounce parameter λ and the total charge Q .

The electric field strength E is obtained as

$$E = \frac{Qr}{(r^2 + \lambda^2)^{3/2}} = E_{\text{RN}} \left[\frac{r^3}{(r^2 + \lambda^2)^{3/2}} \right], \quad (3)$$

with E_{RN} the electric field strength of the RN black hole. One can check it by the Gauss theorem the total charge Q is not totally enclosed in the event horizon due to the absence of the inverse square law of the electric field; actually in the ‘‘charged dust’’ scenario, the BH charge distribution is somewhat diluted, and diffused in the whole spacetime, including outside the horizon, although its density decays very fast in the inverse 6-th power of r [60]. The electromagnetic potential is extracted by integrating the above field and setting the integration constant to zero to ensure the asymptotic flatness, thus we have

$$A_\mu = \frac{Q}{\sqrt{r^2 + \lambda^2}}(1, 0, 0, 0). \quad (4)$$

which is simply a replacement $r \rightarrow \sqrt{r^2 + \lambda^2}$ in the RN electromagnetic potential. As we can see, at a fixed radial coordinate, this spacetime possess weaker electrical potential compared to that of RN case.

A. Regge-Wheeler analysis and the effective potential

The Lagrangian for a charged complex scalar field is given by

$$\mathcal{L} = (D^\nu \Phi)^* D_\nu \Phi + \mu^2 \Phi^* \Phi \quad (5)$$

with $D_\nu = \nabla_\nu + iqA_\nu$ the gauge-covariant derivative chosen to satisfy $[D_\nu, D_\rho] = iqF_{\nu\rho}$, and μ and q the mass and charge of the scalar field respectively. The corresponding Klein-Gordon equation is

$$D_\nu D^\nu \Phi - \mu^2 \Phi = 0. \quad (6)$$

In the time domain, the scalar field admits separable solutions of the form

$$\Phi = \sum_{lm} \frac{\psi(t, r)}{\sqrt{r^2 + \lambda^2}} Y_{lm}(\theta, \phi), \quad (7)$$

where Y_{lm} is spherical harmonic function. The temporal part can be further converted to frequency domain by a Fourier transform $\psi(t, r) = \int d\omega \psi_{\omega l}(r) e^{-i\omega t}$. Substituting these decomposition of componenets into Klein-Gordon equation (6), and invoking the tortoise coordinate x as $dx/dr = 1/f(r)$, we can get the differential equation for the radial part in the time domain,

$$\partial_x^2 \psi - \partial_t^2 \psi - 2iqA_0 \partial_t \psi - [W_{\text{eff}} - (qA_0)^2] \psi = 0, \quad (8)$$

and in the frequency domain,

$$\partial_x^2 \psi_{\omega l} + [(\omega - qA_0)^2 - W_{\text{eff}}] \psi_{\omega l} = 0, \quad (9)$$

with the effective potential W_{eff} explicitly expressed as

$$W_{\text{eff}} = f(r) \left[\frac{l(l+1)}{r^2 + \lambda^2} + \mu^2 + f(r) \frac{\lambda^2}{(r^2 + \lambda^2)^2} + f'(r) \frac{r}{r^2 + \lambda^2} \right] \quad (10)$$

which is a generalization of Regge-Wheeler analysis in [72, 73] with the field charge and mass, in the metric with BH charge and quantum parameter. One can recover the usual RN effective potential by setting $\lambda \rightarrow 0$. Since the effective potential has an intimate relation with the definition of ergo-region [3], which further affects the superradiance magnitude, it is worthwhile to investigate how λ influences the potential. We adopt the definition in [9]: the effective ergo-region is where the quantity below is negative:

$$V_{\text{eff}} = W_{\text{eff}} - (qA_0)^2. \quad (11)$$

This definition singles out terms containing ω in Eq. (9) and is convenient in time-domain analysis which we will carry out later. Here we fix the BH charge to mass ratio to be $Q/M = 0.9$, and choose the field quantities as $qM = 1.4$, $\mu M = 0.3$ and $l = 0$ respectively. We explore the behavior of the effective potential V_{eff} under different values of λ/M as 0.0, 0.4, 0.8 and 1.2, and plot it in Fig.II A.

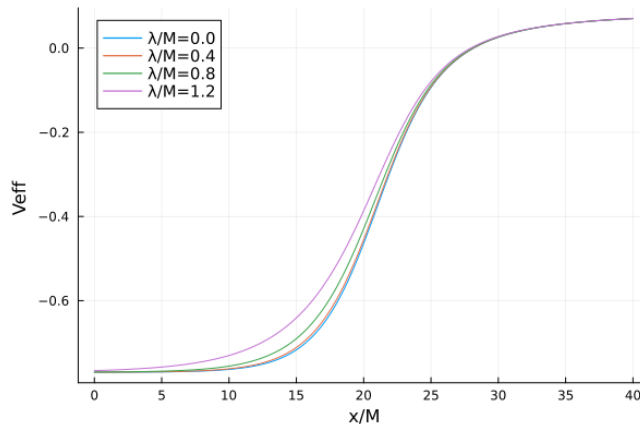


FIG. II. Effective potential for $\mu M = 0.3$, $qM = 1.4$, $Q/M = 0.9$, $l = 0$. Different curves represent different values of λ .

As shown in Fig.II A, the effective potential values at both sides remain identical with different λ and it undergoes a drastic change around $x/M = 20$, while the variation of the effective potential gradually becomes smoother as λ grows larger. As the potential well becomes “shallow”, the extent of negativity a particle’s energy can reach is bounded, thus we could expect, the superradiant ability in the regular background is weakened, as will be confirmed in both the one-time and repeated superradiance process below.

B. The superradiance amplification factor in a scattering experiment

It's useful to consider the asymptotic behaviors of the differential equation (9) to establish a connection between the wave flux at the event horizon and spatial infinity. We assume at infinity there's an incident and reflected wave, nevertheless at the horizon there's only purely ingoing wave, without any quantum-induced reflective part as in [16, 74, 75], thus the solution behaves as

$$\psi_{\omega l} = \begin{cases} \mathcal{I}e^{-ik_{\infty}x} + \mathcal{R}e^{ik_{\infty}x}, & r \rightarrow \infty \\ \mathcal{T}e^{-ik_+x}, & r \rightarrow r_+ \end{cases}, \quad (12)$$

with $k_{\infty} = \sqrt{W_{\text{eff}}} = \sqrt{\omega^2 - \mu^2}$ and $k_+ = \omega - qA_0(r_+)$ the square root of the asymptotic effective potential, and \mathcal{R} , \mathcal{T} the reflection and transmission coefficient respectively. Moreover, due to the conservation of flux (wroskian), we have the relation

$$|\mathcal{R}|^2 + \frac{k_+}{k_{\infty}}|\mathcal{T}|^2 = |\mathcal{I}|^2. \quad (13)$$

It is seen that when $k_+ < 0$, i.e., $\omega < qA_0(r_+)$, the reflection coefficient exceeds the incident coefficient $|\mathcal{R}|^2 > |\mathcal{I}|^2$, which indicates the scalar field is amplified through superradiance and the energy can be extracted from the black hole. A dimensionless amplification factor [3] is defined,

$$Z_l = \left| \frac{\mathcal{R}}{\mathcal{I}} \right|^2 - 1, \quad (14)$$

to measure the effect of superradiance in different choices of parameters. Below we compute it by the numerical methodology commonly employed in the literature [3]. The key is to solve the governing equation (9), in which we impose the purely ingoing boundary condition (12) at a radial coordinate approaching the event horizon, specifically at $r = r_+(1 + \epsilon)$ with $\epsilon = 10^{-5}$ (corrected to 10^{-5}), then we numerically integrate the radial equation (9) starting from the vicinity of the event horizon to a region far from the black hole to determine the solution at $r_{\infty} = 1000r_+$, where the numerical solution has stabilized. The reflection and incident coefficients are identified by comparing it with the asymptotic form derived for $r \rightarrow \infty$ in equation (12), thus the amplification factor is obtained.

It is natural to expect that parameters in both the background and the field could influence this factor, below we focus on the $l = 0$ mode, and specifically choose $\lambda/M = 0.8$, $Q/M = 0.9$, $qM = 1.4$, $\mu M = 0.3$ as our standard value, where the BH mass is used to make other quantities dimensionless. We vary each parameter in the following figures and present our numerical result of the amplification factor as a function of frequency ω in different parameter configurations.

Firstly and importantly, we check the parametric dependence on λ/M , which is the distinct feature of the regular metric. In the left panel of Fig.III, it is seen that with the increase of the quantum parameter λ/M , the magnitude of amplification factor decreases in a wide range of frequencies, as expected in Subsection II A due to the weakening effect on the potential well. More notably, we observe that the reduction rate of the amplification factor exhibits progressive acceleration with successive increasing values of the dimensionless quantum parameter λ/M . Due to the similarity of the overall trend, we also list the dependence on different choices of the scalar field mass μM on the right panel of Fig.III, also we can find that , the amplification factor gradually decreases, in all ranges of ω , with the increasing of μM . But note that numerical solutions are obtained far away from the black hole, the condition $\omega > \mu$ must hold, thus we can observe that all amplified frequencies are greater than the scalar field mass. In both figures, the critical superradiant frequency is $\omega_c M = 0.8775$, which is not affected by λ/M and μM .

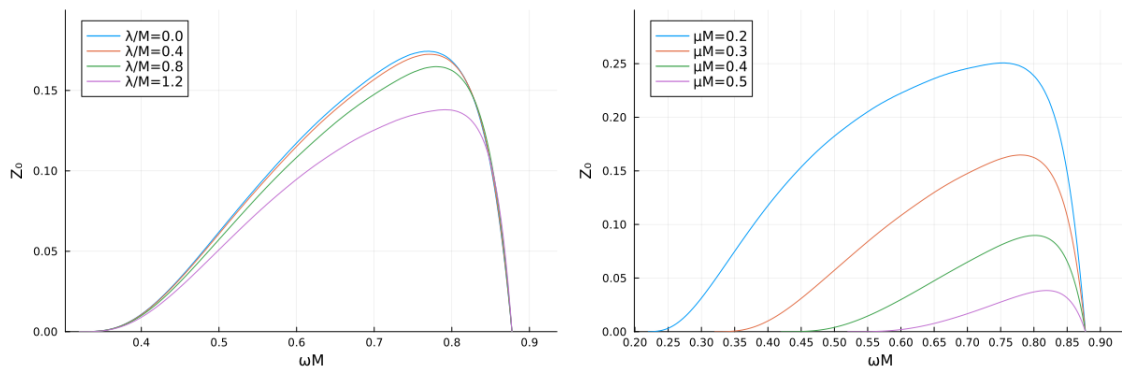


FIG. III. Amplification factor of the scalar field as a function of the frequency with dependence on different choices of λ/M (left) and on different field mass μM (right). Curves in blue, orange, green, purple color in the left panel denote cases of $\lambda/M = 0, 0.4, 0.8, 1.2$ respectively with $\mu M = 0.3$ fixed, and in the right panel denote $\mu M = 0.2, 0.3, 0.4, 0.5$ respectively with $\lambda/M = 0.8$ fixed. Other parameters are chosen as as the standard values, $Q/M = 0.9, qM = 1.4, l = 0$. The point where curves meet the horizontal axis gives the critical superradiant frequency, which is $\omega_c M = 0.8775$ in these cases.

Another group of parameters are the BH and the field charge, which do affect the critical superradiant frequency as $\omega = qA_0$, as the increase of the charges leads to substantial broadening of the cutoff frequency range. We present the dependence of the amplification factor on Q/M and qM on the left and right panels of Fig.IV. We can find a similar trend that with the increases of the BH or field charge, the amplification factor decreases in the low-frequency regime, but increased in the high-frequency

regime.

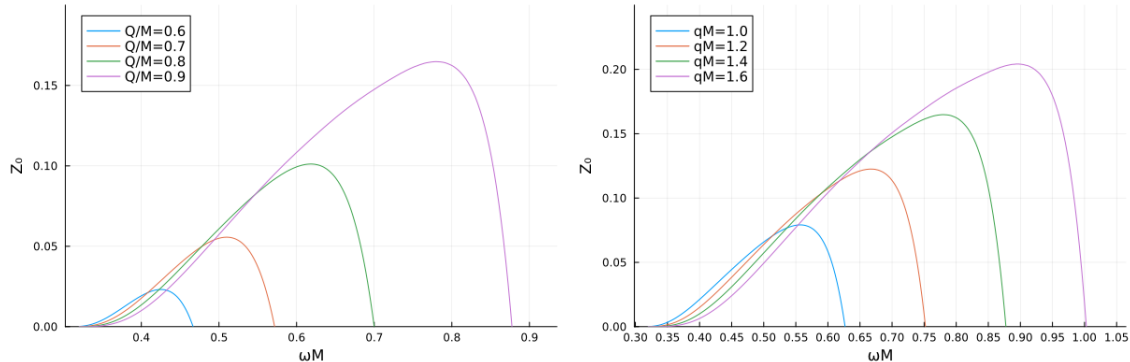


FIG. IV. Amplification factor of the scalar field as a function of the frequency with dependence on different choices of Q/M (left) and on different field mass qM (right). Curves in blue, orange, green, purple color in the left panel denote cases of $Q/M = 0.6, 0.7, 0.8, 0.9$ respectively with $qM = 1.4$ fixed, and in the right panel denote $qM = 1, 1.2, 1.4, 1.6$ respectively with $Q/M = 0.9$ fixed. Other parameters are chosen as the standard values, $\lambda/M = 0.8, \mu M = 0.3, l = 0$.

In the above analysis, the quasi-stationary approximation is implied, i.e., fluctuations of order $\mathcal{O}(\epsilon)$ in the scalar field in the background induce changes in the spacetime geometry of order $\mathcal{O}(\epsilon^2)$, due to the fact that the stress-energy tensor is quadratic in the fields, and therefore to leading order can be studied on a fixed geometry [3]. Up to now, we have discussed the parameter dependence of a regular BH to the superradiant scattering amplification factor. The main ingredient is coded in the effective potential. Later we will see this also holds in the case of a BH bomb scenario.

III. BLACK HOLE BOMBS OF TYPE I AND II IN BLACK-BOUNCE-REISSNER-NORDSTRÖM SPACETIMES

As we've mentioned in the introduction, a scenario where a black hole is enclosed by reflective mirrors, the superradiant mechanism can induce amplification of scalar fields confined between the event horizon and the mirror boundary. The field mass in the Kerr metric could serve as a natural mirror, while in RN due to the stability of the spacetime only theoretical reflective boundary condition can be used to confine the field. This energy accumulation in the scalar field may eventually breaks the mirror, leading to the black hole bomb phenomenon [7]. This section aims to numerically investigate black hole bombs on the black-bounce-RN black hole. The definition of the conserved energy should be firstly given.

A. The energy current for the charged scalar field

The symmetric energy-momentum tensor $T_{\rho\nu}$ for the charged scalar field corresponding to the Lagrangian (5) is given by

$$T_{\rho\nu} = D_{(\rho}\Phi(D_{\nu)}\Phi)^* - g_{\rho\nu}\mathcal{L}. \quad (15)$$

which is not divergence-less due to the exclusion of the background electro-magnetic term in the Lagrangian, physically the coupling back is ignored [9, 30]. Hence the energy current $J_\rho \equiv T_{\rho 0}$ is not conserved and the covariant derivative is explicitly given as

$$\nabla_\nu J^\nu = qF_{\nu 0}(\phi_2\nabla^\nu\phi_1 - \phi_1\nabla^\nu\phi_2), \quad (16)$$

where ϕ_1 and ϕ_2 represent the real and imaginary part of scalar field. Via eliminating the electric potential from the energy current we can construct a conserved energy current, which encodes the intrinsic energy of the scalar field. The conserved energy current reads

$$J_{\nu,c} = \sum_{j=1,2} \left[\partial_\nu\phi_j\partial_t\phi_j - \frac{1}{2}\mu^2 g_{\nu 0}\phi_j^2 - \frac{1}{2}g_{\nu 0}g^{\rho\sigma}(\partial_\rho\phi_j\partial_\sigma\phi_j + q^2 A_\rho A_\sigma\phi_j^2) \right]. \quad (17)$$

which shares the same form as the RN black hole [9]. Through the energy current, we can also construct the energy flux at a fixed radial distance, by integrating the $\nu = 1$ component of Eq. (18),

$$\mathcal{F}_r = \int (r^2 + \lambda^2) dt d\theta d\varphi \operatorname{Re}(\partial_t\Phi\partial_x\Phi^*). \quad (18)$$

Substituting Eq. (7) into Eq. (18), we obtain

$$\mathcal{F}_r = \frac{1}{2} \int dt (\partial_t\psi\partial_x\psi^* + \partial_t\psi^*\partial_x\psi), \quad (19)$$

where the normalization of spherical harmonic functions $\int_0^\pi d\theta \int_0^{2\pi} d\varphi \sin\theta Y_{lm}(\theta, \varphi)Y_{lm}^*(\theta, \varphi) = 1$ is used. The Eqs. (18) and (19) measures energy that across a hypersurface where x is a constant. Suppose we place this hypersurface near the event horizon, since only the incident waves that fall into the black hole are involved, we can calculate the negative energy passing through, and equivalently we obtain the energy gain of the scalar field according to the energy conservation.

B. Numerical methods and boundary conditions

Here we present the numerical strategy to solve the partial differential equation (8) in the time domain, where we adopt the finite difference method combined with the method of lines. First, we

uniformly discretize the spatial coordinates with a grid spacing of δx . Therefore, the spatial derivatives after discretization can be expressed as

$$\partial_x \psi = \frac{\psi_{i+1} - \psi_{i-1}}{2\delta x}, \quad (20)$$

$$\partial_x^2 \psi = \frac{\psi_{i+1} - 2\psi_i + \psi_{i-1}}{\delta x^2}, \quad (21)$$

where ψ_i denotes $\psi(t, x_m - i \times \delta x)$ and x_m is the mirror's position. After discretizing the spatial coordinates, we obtain a system of ordinary differential equations (ODEs) containing only time derivatives. We employ the fourth-order Runge-Kutta method to numerically integrate this system of ODEs, where we set $\delta x/M = 0.2$ in the computation.

For a black bomb, since all waves at the mirror are completely reflected back, the boundary condition at the mirror surface can be simply represented as a Dirichlet boundary condition, namely that the value of the solution is set to vanish, corresponding to $\psi(t, x_m) = 0$. Another boundary condition occurs at the horizon, however since the tortoise coordinate spans from $-\infty$ to x_m , truncating the computational domain at the left becomes necessary. Due to the fact that applying Dirichlet or Neumann boundary conditions directly at the truncated boundaries introduces artificial wave reflections, we employ the technique of Perfectly Matched Layers (PML) boundary [67] to suppress outgoing waves effectively, in which an absorbing region at the computational boundary is introduced, so that outgoing waves are attenuated through damping profiles.

To ensure the simplicity of the equation after applied the PML, we first change the variable to $\psi = e^{i(qA_0 + \sqrt{W_{\text{eff}}})t} u(t, x)$, then we obtain

$$\partial_t^2 u - \partial_x^2 u + 2i\sqrt{W_{\text{eff}}}\partial_t u = 0. \quad (22)$$

In the frequency domain, the time derivative is replaced by $-i\omega$. By further applying the substitution $\partial_x^2 \rightarrow \frac{1}{1+i\sigma(x)/\omega}\partial_x^2$, we obtain the modified partial differential equation compatible with the PML framework in the frequency domain

$$(-i\omega)^2 u - \partial_x^2 u + 2i\sqrt{W_{\text{eff}}}(-i\omega)u + \sigma(x)(-i\omega)u + 2i\sigma(x)\sqrt{W_{\text{eff}}}u = 0, \quad (23)$$

where $\sigma(x)$ is defined as continuous function that vanishes in the physical domain outside the absorbing layer and assumes non-zero values only within the absorbing region. To eliminate wave reflections at the interface between the physical domain and the absorbing layer, $\sigma(x)$ must be carefully formulated as a smoothly varying function to guarantee effective wave attenuation. Transforming the above equation

(23) from the frequency domain back to the time domain, the equation becomes

$$\partial_t^2 u - \partial_x^2 u + \sigma \partial_t u + 2i\sqrt{W_{\text{eff}}}\partial_t u + 2i\sigma\sqrt{W_{\text{eff}}}u = 0. \quad (24)$$

Changing the variables to ψ , we get

$$\partial_t^2 \psi - \partial_x^2 \psi - 2iqA_0\partial_t \psi + V_{\text{eff}}\psi + \sigma\partial_t \psi + i\sigma(\sqrt{W_{\text{eff}}} - qA_0)\psi = 0. \quad (25)$$

When $\sigma(x) = 0$, Eq.(25) reduces to the original partial differential equation (8), demonstrating that the presence of $\sigma(x)$ preserves the intrinsic wave dynamics within the physical domain. Conversely, in regions where $\sigma \neq 0$ (within the absorbing layer), the modified equation (25) incorporates three dissipative terms, leading to exponential attenuation of wave amplitudes until complete extinction occurs. This ensures that outgoing waves are absorbed without contaminating the physical domain. Note that our substitution scheme modifies the second spatial derivative as $\partial_x^2 \rightarrow \frac{1}{1+i\sigma(x)/\omega}\partial_x^2$, rather than the conventional first-order derivative replacement $\partial_x \rightarrow \frac{1}{1+i\sigma(x)/\omega}\partial_x$. This approach leverages the combined dissipative and damping terms to suppress reflections when a sufficiently thick absorption layer is implemented. In contrast, adopting the standard substitution would introduce prohibitive complexity into the resulting modified partial differential equation.

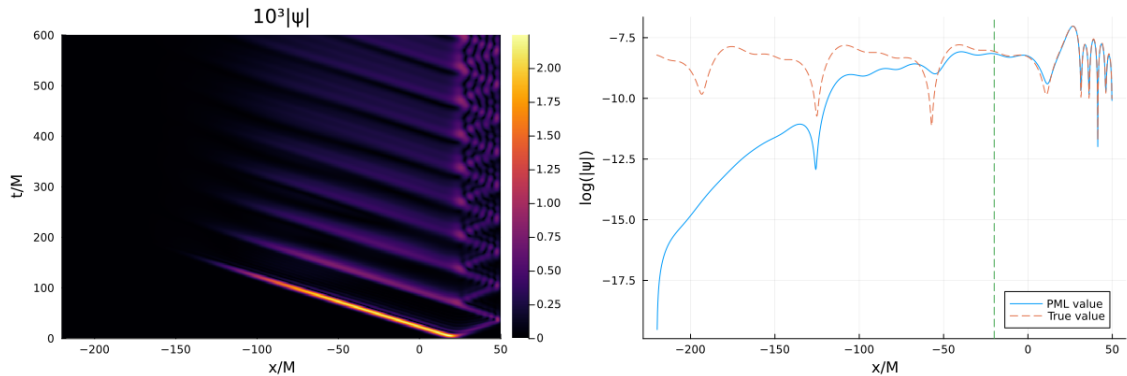


FIG. V. The validation of the effectiveness of PML boundary condition. The left panel illustrates the continuous reflection and transmission of the scalar field between the mirror and the black hole. The right panel presents a comparison between the scalar field amplitude after applying PML boundary conditions and the true amplitude. The dash green line is the boundary of the PML layer.

Next, we evaluate the efficacy of PML boundary conditions. This verification involves two key aspects: first, ensuring that no reflected waves are generated either at the boundary or within the absorbing layer itself; second, confirming whether the absorbing layer fully attenuates the incoming

waves. We set the truncation boundary at $x_0 = -20M$ with a PML layer width of $200M$. The initial condition is defined as a Gaussian wave packet

$$\begin{cases} \psi(t = 0, x) = \psi_0 e^{-(x-x_{\text{in}})^2/\alpha^2}, \\ \partial_t \psi(t = 0, x) = 0, \end{cases} \quad (26)$$

with ψ_0 the peak amplitude of the wave packet, x_{in} its initial center position, and α the spatial width of the wave packet. We set $\psi_0 = 10^{-3}$, $\alpha = 5M$ to include as many frequency components as possible and choose the initial position to be $x_{\text{in}} = 20M$, where the effective potential is sharpest, as shown in Fig.II A. We present the validation results in Fig.V. The left panel demonstrates that the incident wave undergoes transmission and reflection at the initial place, with the part incident into the absorbing layer gradually diminish until completely disappearing, while the other part on the right side are fully reflected back at the mirror. The right panel shows the wave amplitude at $t = 600M$, where it can be observed that the application of the PML boundary condition does not affect the values within the physical domain.

C. Evolution of the scalar field and impact of the regularization parameter

We proceed to study the evolution of the scalar field in the first two cases mention in [30]: Type I, the mirror's position is set outside the effective ergosphere; Type II, the mirror's position is set inside the effective ergosphere. When extracting the eigenfrequencies of scalar field, we employ the fast fourier transform (FFT) to obtain the real parts and utilize digital filter method to extract the imaginary parts of the eigenfrequencies. To measure the energy gain of the scalar field, we adopt Eq. (18) to numerically calculate it.

In a Type I BH bomb, we position the mirror outside the ergosphere at $x_m = 50M$, and set the absorbing layer to span from $x = -50M$ to $x = -250M$. The parameters in effective potential are taken as $Q/M = 0.9$, $\mu M = 0.3$, $qM = 1.4$ and $l = 0$, with the critical superradiant frequency $\omega_c = qA_0(r_+) = 0.8775/M$. The initial condition is set by a Gaussian wave packet described by Eq. (26), with $\psi_0 = 10^{-3}$, $x_{\text{in}} = 20M$ and $\alpha = 5M$. Additionally, the energy flux at $x_s = -40M$ is also measured. The results are shown in the Fig.VI, with three columns from the left to right, representing the real part of amplitude, power spectral and energy flux, respectively. From top to bottom panels, the corresponding values of λ/M are taken as 0.0, 0.8 and 1.2 respectively. The eigenfrequencies corresponding to the power spectrum in the middle column are listed in table II. It is observed that the

wave amplitude, the real and imaginary parts of the eigenfrequencies and energy flux simultaneously decrease with the increase of λ . Especially, as shown in the bottom plots in Fig. VI, the real part of the fourth eigenfrequency decreases sufficiently to meet the superradiant condition, resulting in a new distinct growing modes at this configuration, though the amplification of the scalar field remains diminished due to the reduced imaginary part of the eigenfrequencies.

In a Type II BH bomb, the scalar field undergoes reflection and transmission between the mirror and the boundary of the ergo-region. We place the mirror within the ergosphere at $x_m = -10M$, other parameters chosen as the same as in Type I, while we measure the energy flux at $x_s = 70M$ in this case. Yet, there are still two situations in this scenario, when the superradiance frequency exceeds the scalar field mass $\omega_c > \mu$, there could exist the eigenfrequencies ω lies between them, allowing the field to propagate outward through the boundary of the ergoregion; conversely, when the field's mass exceeds the superradiant eigenfrequency $\mu > \omega_c$, there's also a chance for eigenfrequencies that satisfy $\omega < \omega_c$, rendering the field confined within the ergoregion, to form a persistent scalar cloud surrounding the black hole. The evolutions of the scalar field in these two subcases are shown in Fig.VII, where it is obviously seen that the waves appear outside the effective potential when $\omega_c > \omega > \mu$ and disappear when $\mu > \omega_c > \omega$.

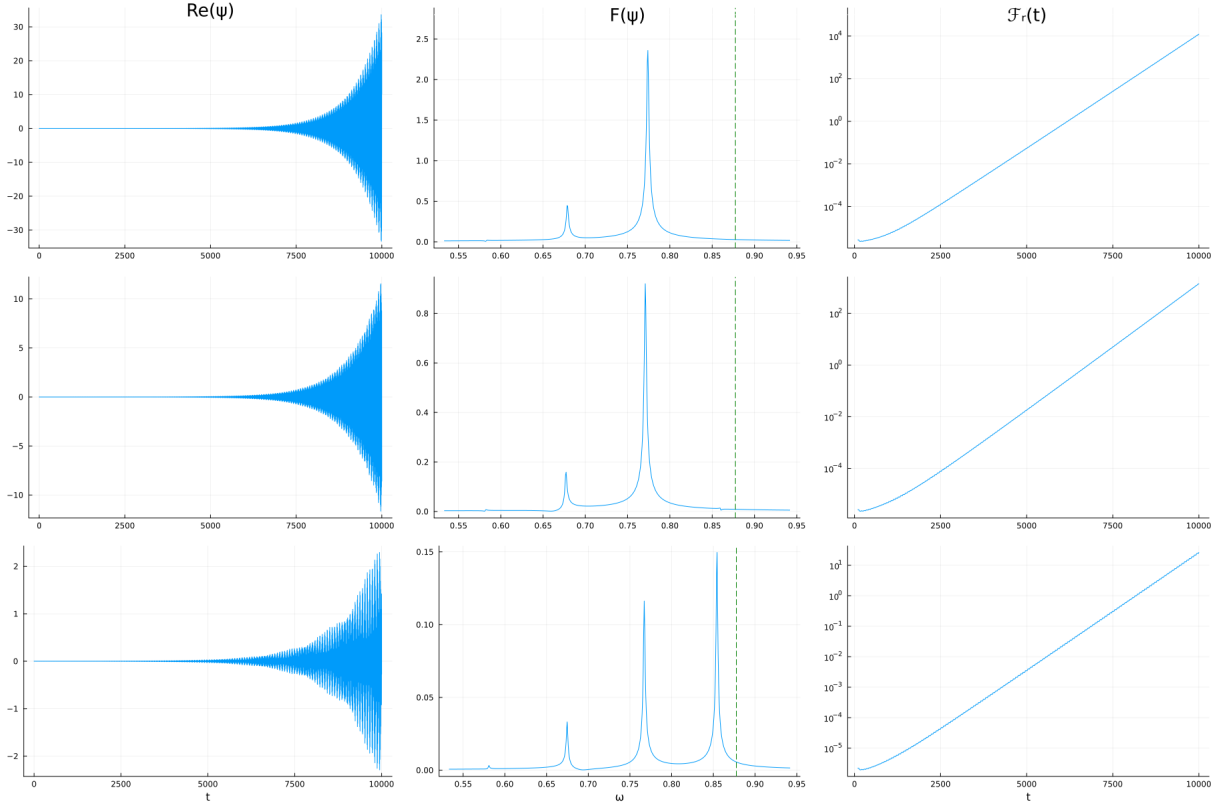


FIG. VI. Evolution of the scalar field in a Type I BH bomb. The position of the mirror is at $x_m = 50M$, and the parameters are set as $Q/M = 0.9$, $\mu M = 0.3$, $qM = 1.4$, $l = 0$. From left to right, the three columns represent the field amplitude, power spectrum and energy flux (measured at $x_s = -40M$). From top to bottom, the values of λ/M are 0.0, 0.8 and 1.2 respectively. The green dash line represents the critical superradiant frequency which is approximately $\omega_c M \simeq 0.8775$.

λ/M	$\omega_0 M$	$\omega_1 M$	$\omega_2 M$	$\omega_3 M$
0.0	$0.5831 + i8.073 \times 10^{-4}$	$0.6785 + i1.125 \times 10^{-3}$	$0.7740 + i1.243 \times 10^{-3}$	/
0.8	$0.5818 + i7.319 \times 10^{-4}$	$0.6773 + i1.014 \times 10^{-3}$	$0.7709 + i1.138 \times 10^{-3}$	/
1.2	$0.5811 + i6.243 \times 10^{-4}$	$0.6747 + i8.388 \times 10^{-4}$	$0.7671 + i9.094 \times 10^{-4}$	$0.8544 + i9.832 \times 10^{-4}$

TABLE II. Numerics of eigenfrequencies in a Type I BH bomb, corresponding to the middle panel of Fig. VI, both the real and imaginary parts are presented. The table is divided with respect to different choices of the quantum parameter λ/M . Three modes appear in the $\lambda/M = 0, 0.8$ case, while a new eigen-mode show up in the $\lambda/M = 1.2$ case.

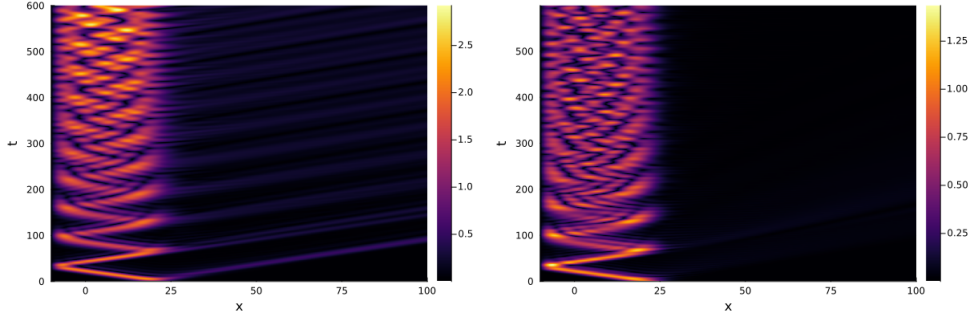


FIG. VII. Spacetime diagram of the field strength evolution in a Type II BH bomb, with the mirror setting at $x_m = -10M$, and the PML ranging from $100M - 300M$. The sub-case of light particles ($\mu < \omega_c$) is shown on the left, with a parameter choices of $\mu M = 0.3$, $Q/M = 0.9$, $qM = 1.0$ and $\omega_c M = 0.8775$; while the sub-case of heavy particles ($\mu > \omega_c$) is shown on the right, with the choice of $\mu M = 0.6$, $Q/M = 0.9$, $qM = 0.8$ and $\omega_c = 0.5014$.

For $\omega_c > \mu$, we also present the field evolution in Fig.IX. Again, as λ increases, both the scalar field amplitudes and energy fluxes exhibit monotonic decrease, and so do the imaginary parts of the eigenfrequencies. Numerics corresponding to the eigenvalues are shown in Table III, where there's only two eigen-modes and no new modes appearing in the $\lambda/M = 1.2$ case, different from that in Type I BH bomb.

For $\mu > \omega_c$, we set $\mu M = 0.6$, $Q/M = 0.9$, $qM = 0.8$, and the value of λ are taken as 0.0 and 1.2, thus the corresponding superradiant frequency is $\omega_c = 0.5014$. The evolutions are shown in Fig.VIII, where wave amplifications are absent, yet eigen-frequencies are drawn in the right panel. Compared with the case where $\lambda = 0.0$, when $\lambda = 1.2$, there exist a new eigen-frequencies within the range of $\omega < \omega_c$.

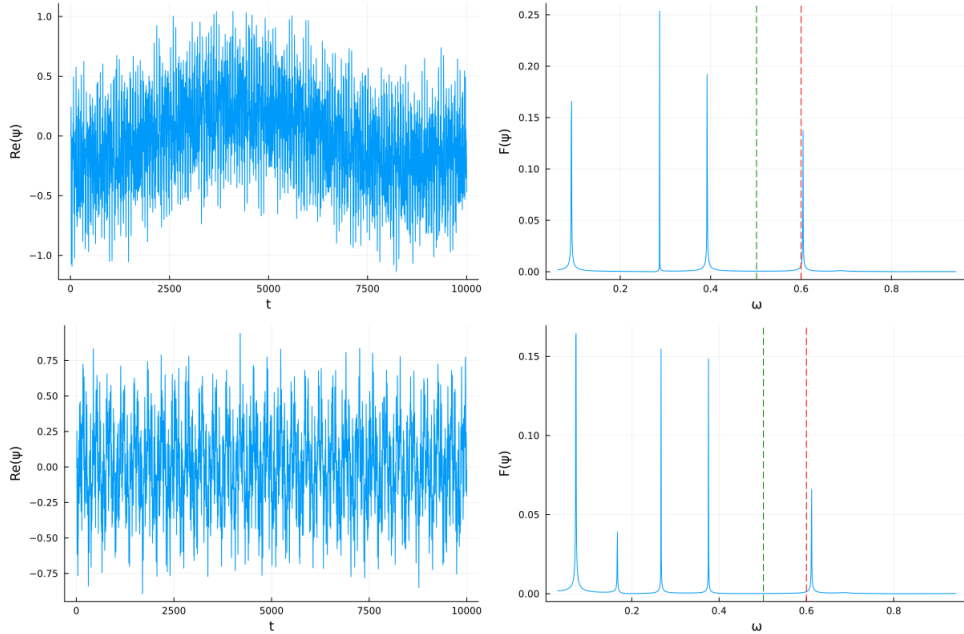


FIG. VIII. Evolution of the scalar field in the sub-case of $\mu > \omega_c$ in a Type II BH bomb. The wave amplitude evolution measured at $x = 0$ is shown on the left and the corresponding power spectrum is shown on the right, with $\mu M = 0.6$ denoted by the red dashed line and $\omega_c \simeq 0.5$ by the green dashed line. Other parameters are chosen as $Q/M = 0.9$, $qM = 0.8$, $\lambda/M = 0.0$ (Top) and 1.2 (Bottom).

λ/M	$\omega_0 M$	$\omega_1 M$
0.0	$0.6672 + i1.234 \times 10^{-3}$	$0.7721 + i1.485 \times 10^{-3}$
0.8	$0.6609 + i1.095 \times 10^{-3}$	$0.7683 + i1.428 \times 10^{-3}$
1.2	$0.6477 + i0.929 \times 10^{-3}$	$0.7583 + 1.235 \times 10^{-3}$

TABLE III. Numerics of eigenfrequencies in a Type II BH bomb, corresponding to the middle panel of Fig. IX, both the real and imaginary parts are presented. The table is divided with respect to different choices of the quantum parameter λ/M . In this sub-case, two distinct modes emerge across the three specified values of λ/M .

IV. CONCLUSION

In this work, we studied the superradiance for a charged scalar field propagating in the spacetime of a black-bounce-RN black hole, which could be obtained by the replacement $r \rightarrow \sqrt{r^2 + \lambda^2}$ in the

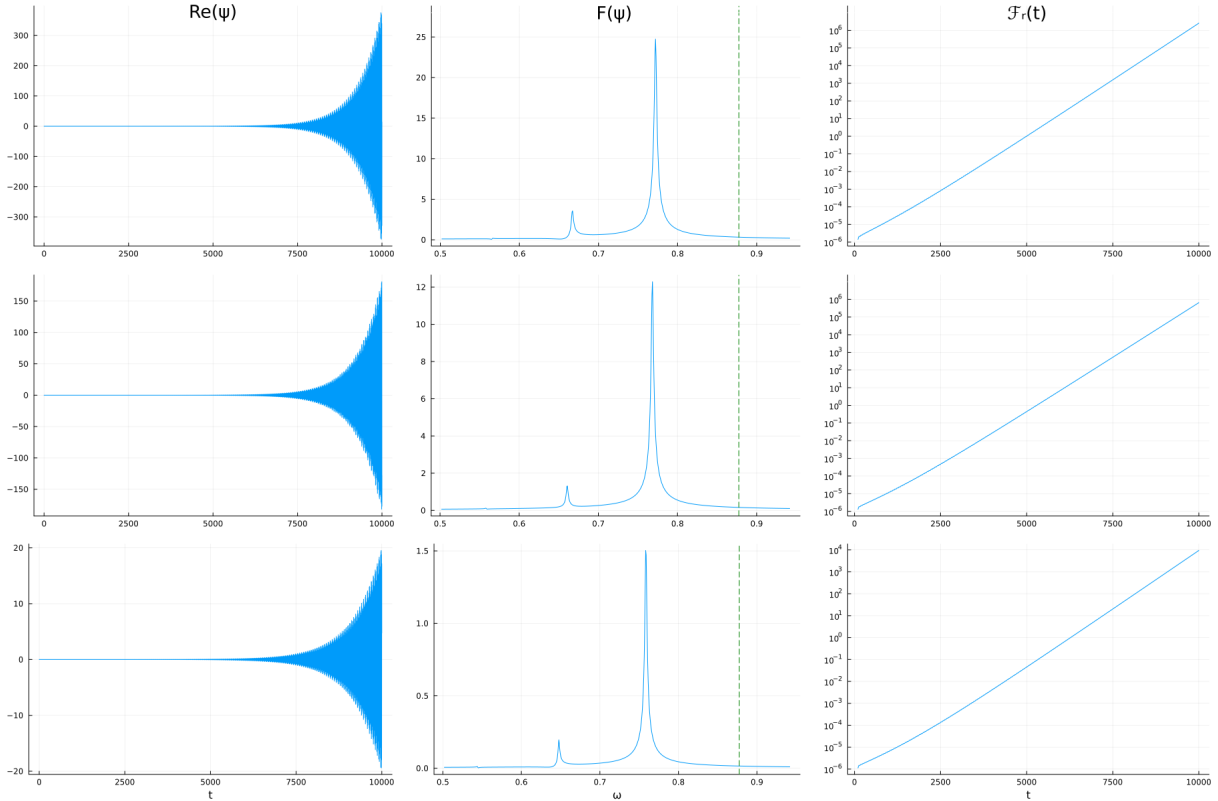


FIG. IX. Evolution of the scalar field in a Type II BH bomb, in the sub-case of light particles $\mu < \omega_c$. The position of the mirror is at $x_m = -10M$, and the parameters are set as $Q/M = 0.9$, $\mu M = 0.3$, $qM = 1.4$, $l = 0$. From left to right, the three columns represent the field amplitude, power spectrum and energy flux (measured at $x_s = 70M$). From top to bottom, the values of λ/M are 0.0, 0.8 and 1.2 respectively. The green dash line represents the critical superradiant frequency which is approximately $\omega_c M \simeq 0.8775$.

RN metric to reduce the curvature singularity. The existence of the quantum parameter λ shallowed the effective potential in the Regge-Wheeler equation hence weakened the negativity of the energy a field/particle can get, which further reduce the superradiant abilities both in the scattering experiment and the BH bomb phenomenon. We verified the effect in these two scenario numerically and found several new features that may provide insights to related research.

In the superradiant scattering experiment, we focused on the influence that parameters had on the amplification factor defined as $Z = |\mathcal{R}|^2 / |\mathcal{I}|^2 - 1$. As expected, numerical results reveal that the quantum parameter λ indeed reduced the amplification factor over the whole frequency range, which indicates that black-bounce-RN BH has a weaker superradiant amplification than the usual RN BH. In a similar manner, the larger field mass suppresses the amplification in all frequencies, in agreement

with the physical intuitive that heavier particles are dominated more by the gravitational attraction and harder to decay/transit into negative energy states. Another pair of parameters, the BH and the field charge, affect the amplification factor in a coherent way, they raised the critical frequency as the superradiant condition indicates, and notably enhance it at high frequencies while suppress it in low frequencies, which are consistent with the behaviors observed in the RN BH case as they are independent of the quantum parameter.

In the black hole bomb phenomenon, we investigated in the time domain the evolution of the charged scalar field in a fixed background of black-bounce RN BH, subjected to the mirror-like boundary condition. In two types of BH bombs, where mirror is set without or within the ergoregion, the amplitude evolution, the eigenfrequencies and the energy growth rate are simulated. Technically, we employed the finite difference method combined with the method of lines to numerically solve the differential equation for the field amplitude evolution. The Dirichlet boundary condition is chosen at the mirror to fully reflect the wave, while the purely ingoing boundary condition at the event horizon is implemented by the Perfectly Matched Layers, which validity was tested in our numerical simulations. The eigenfrequencies were extracted by the discrete fourier transform and digital filter method. To measure the energy flux, we constructed analytically a conserved energy current based on the stress-energy tensor of the scalar field, and invoke the numerical values obtained to achieve it. Again as expected, the wave amplification and the energy growth rate is weakened by a larger value of the quantum number. However, we discovered that in the Type I BH bomb case when $\lambda/M = 1.2$ a new distinct eigen-mode appeared while in the Type II BH bomb case there's no such an extra mode, compared to those of $\lambda/M = 0, 0.8$. The mathematical observation attribute this to a decrease of the real part of the frequency, but the physical origin deserves a further analytical study in the future. Moreover, in the case of Type II bomb, we investigated further when the field mass is larger than the critical frequency $\mu > \omega_c$, finding that wave amplifications are absent in the confinement scenario. Consistent with the Type I BH bomb case, a new eigen-mode emerges under the $\lambda = 1.2$ condition when compared to the $\lambda = 0.0$ configuration.

The study is straightforward to be extended to several directions. First, in current paper, we only focus on the influence of quantum parameter in the spherically symmetric charged black bounce black hole. In contrast to it, the effects of quantum parameters in nonsingular rotating black hole configurations have yet to be systematically investigated. This will advance our understanding of how quantum parameter governs superradiant energy extraction processes and black hole bomb instability. Moreover, the present study employs an artificially engineered reflecting boundary condition beyond the event

horizon to constrain the scalar field. Nevertheless, the implementation through nonlinear interaction terms within the scalar field framework provides an alternative pathway to achieve analogous confinement effects [76]. In addition, this investigation confines its scope to evolution of scalar field, while further studies are needed to explore the dynamics of black hole mass and charge.

ACKNOWLEDGEMENTS

The work of Xiangdong Zhang is supported by the National Natural Science Foundation of China with Grant No. 12275087. The work of Gui-Rong Liang is supported by the National Natural Science Foundation of China with Grant No. 12175099 and Jiangsu Funding Program for Excellent Postdoctoral Talent with No. 2024ZB752.

-
- [1] O. Klein, *Die reflexion von elektronen an einem potentialsprung nach der relativistischen dynamik von dirac*, *Zeitschrift für Physik* **53** (1929) 157.
 - [2] F. Sauter, *Über das verhalten eines elektrons im homogenen elektrischen feld nach der relativistischen theorie diracs*, *Zeitschrift für Physik* **69** (1931) 742.
 - [3] R. Brito, V. Cardoso and P. Pani, *Superradiance: New Frontiers in Black Hole Physics*, Springer International Publishing (2020), [10.1007/978-3-030-46622-0](https://doi.org/10.1007/978-3-030-46622-0).
 - [4] C.A. Manogue, *The klein paradox and superradiance*, *Annals of Physics* **181** (1988) 261.
 - [5] R. Penrose, *Gravitational collapse: The role of general relativity*, *Riv. Nuovo Cim.* **1** (1969) 252.
 - [6] S.A. Teukolsky and W.H. Press, *Perturbations of a rotating black hole. iii - interaction of the hole with gravitational and electromagnetic radiation*, *Astrophys. J.* **193** (1974) 443.
 - [7] W.H. Press and S.A. Teukolsky, *Floating orbits, superradiant scattering and the black-hole bomb*, *Nature* **238** (1972) 211.
 - [8] G. Denardo and R. Ruffini, *On the energetics of reissner nordström geometries*, *Phys. Lett. B* **45** (1973) 259.
 - [9] L.D. Menza and J.-P. Nicolas, *Superradiance on the reissner–nordström metric*, *Classical and Quantum Gravity* **32** (2015) 145013.
 - [10] S. Hod, *Stability of the extremal reissner–nordström black hole to charged scalar perturbations*, *Physics Letters B* **713** (2012) 505.
 - [11] S. Hod, *No-bomb theorem for charged reissner–nordström black holes*, *Physics Letters B* **718** (2013) 1489.
 - [12] W.H. PRESS and S.A. TEUKOLSKY, *Floating orbits, superradiant scattering and the black-hole bomb*, *Nature* **238** (1972) 211.

- [13] W.E. East and F. Pretorius, *Superradiant instability and backreaction of massive vector fields around kerr black holes*, *Physical Review Letters* **119** (2017) .
- [14] S. Endlich and R. Penco, *A modern approach to superradiance*, *Journal of High Energy Physics* **2017** (2017) .
- [15] S.R. Dolan, *Superradiant instabilities of rotating black holes in the time domain*, *Physical Review D* **87** (2013) .
- [16] N. Jia, Y.-D. Guo, G.-R. Liang, Z.-F. Mai and X. Zhang, *Superradiant growth anomaly magnification in evolution of vector bosonic condensates bounded by a kerr black hole with near-horizon reflection*, *Sci. China Phys. Mech. Astron.* **68** (2025) 240411 [2309.05108].
- [17] W.E. East and F. Pretorius, *Superradiant instability and backreaction of massive vector fields around kerr black holes*, *Phys. Rev. Lett.* **119** (2017) 041101.
- [18] S.R. Dolan, *Instability of the massive klein-gordon field on the kerr spacetime*, *Phys. Rev. D* **76** (2007) 084001.
- [19] J.-H. Huang, W.-X. Chen, Z.-Y. Huang and Z.-F. Mai, *Superradiant stability of the kerr black holes*, *Physics Letters B* **798** (2019) 135026.
- [20] E. Franzin, S. Liberati and M. Oi, *Superradiance in kerr-like black holes*, *Physical Review D* **103** (2021) .
- [21] M. Khodadi and R. Pourkhodabakhshi, *Superradiance and stability of kerr black hole enclosed by anisotropic fluid matter*, *Physics Letters B* **823** (2021) 136775.
- [22] J.-H. Huang, W.-X. Chen, Z.-Y. Huang and Z.-F. Mai, *Superradiant stability of the kerr black holes*, *Physics Letters B* **798** (2019) 135026.
- [23] T. Kobayashi and A. Tomimatsu, *Superradiant scattering of electromagnetic waves emitted from disk around kerr black holes*, *Physical Review D* **82** (2010) .
- [24] Z. Li, *Superradiance and quasinormal modes of the gravitational perturbation around rotating hairy black hole*, *Physics Letters B* **841** (2023) 137902.
- [25] G. Mascher, K. Destounis and K.D. Kokkotas, *Charged black holes in de sitter space: Superradiant amplification of charged scalar waves and resonant hyperradiation*, *Physical Review D* **105** (2022) .
- [26] C.L. Benone, E.S. de Oliveira, S.R. Dolan and L.C. Crispino, *Absorption of a massive scalar field by a charged black hole*, *Physical Review D* **89** (2014) .
- [27] C.L. Benone and L.C. Crispino, *Superradiance in static black hole spacetimes*, *Physical Review D* **93** (2016) .
- [28] Z. Zhu, S.-J. Zhang, C. Pellicer, B. Wang and E. Abdalla, *Stability of reissner-nordström black hole in de sitter background under charged scalar perturbation*, *Physical Review D* **90** (2014) .
- [29] R.A. Konoplya and A. Zhidenko, *Charged scalar field instability between the event and cosmological horizons*, *Phys. Rev. D* **90** (2014) 064048 [1406.0019].

- [30] L. Di Menza, J.-P. Nicolas and M. Pellen, *A new type of charged black hole bomb*, *General Relativity and Gravitation* **52** (2020) .
- [31] N. Sanchis-Gual, J.C. Degollado, P.J. Montero, J.A. Font and C. Herdeiro, *Explosion and final state of an unstable reissner-nordström black hole*, *Phys. Rev. Lett.* **116** (2016) 141101.
- [32] C.A.R. Herdeiro, J.C. Degollado and H.F. Rúnarsson, *Rapid growth of superradiant instabilities for charged black holes in a cavity*, *Phys. Rev. D* **88** (2013) 063003 [1305.5513].
- [33] J.C. Degollado, C.A.R. Herdeiro and H.F. Rúnarsson, *Rapid growth of superradiant instabilities for charged black holes in a cavity*, *Physical Review D* **88** (2013) .
- [34] N. Sanchis-Gual, J.C. Degollado, P.J. Montero, J. Font and C. Herdeiro, *Explosion and final state of an unstable reissner-nordström black hole*, *Physical Review Letters* **116** (2016) 141101.
- [35] N. Sanchis-Gual, J.C. Degollado, C. Herdeiro, J. Font and P.J. Montero, *Dynamical formation of a reissner-nordström black hole with scalar hair in a cavity*, *Physical Review D* **94** (2016) 044061.
- [36] S.R. Dolan, S. Ponglertsakul and E. Winstanley, *Stability of black holes in einstein-charged scalar field theory in a cavity*, *Physical Review D* **92** (2015) 124047.
- [37] S.S. Gubser, *Breaking an abelian gauge symmetry near a black hole horizon*, *Physical Review D* **78** (2008) 065034.
- [38] S.A. Hartnoll, C.P. Herzog and G.T. Horowitz, *Building a holographic superconductor*, *Physical Review Letters* **101** (2008) 031601.
- [39] S. Hod, *Analytic treatment of the charged black-hole-mirror bomb in the highly explosive regime*, *Physical Review D* **88** (2013) .
- [40] R. Li, J.-K. Zhao and Y.-M. Zhang, *Superradiant instability of d-dimensional reissner—nordström black hole mirror system**, *Communications in Theoretical Physics* **63** (2015) 569.
- [41] J.C. Degollado, C.A.R. Herdeiro and H.F. Rúnarsson, *Rapid growth of superradiant instabilities for charged black holes in a cavity*, *Physical Review D* **88** (2013) 063003.
- [42] J.C. Degollado and C.A.R. Herdeiro, *Time evolution of superradiant instabilities for charged black holes in a cavity*, *Physical Review D* **89** (2014) 063005.
- [43] O.J.C. Dias and R. Masachs, *Charged black hole bombs in a minkowski cavity*, *Classical and Quantum Gravity* **35** (2018) 184001.
- [44] R. Li and J. Zhao, *Numerical study of superradiant instability for charged stringy black hole–mirror system*, *Physics Letters B* **740** (2015) 317.
- [45] R. Li, Y. Tian, H. Zhang and J. Zhao, *Time domain analysis of superradiant instability for the charged stringy black hole–mirror system*, *Physics Letters B* **750** (2015) 520.
- [46] H. Furuhashi and Y. Nambu, *Instability of massive scalar fields in kerr-newman spacetime*, *Progress of Theoretical Physics* **112** (2004) 983
[<https://academic.oup.com/ptp/article-pdf/112/6/983/5395014/112-6-983.pdf>].

- [47] A. Ashtekar, J. Olmedo and P. Singh, *Regular black holes from loop quantum gravity*, [2301.01309](#).
- [48] J. Bardeen, *Non-singular general relativistic gravitational collapse*, .
- [49] S.A. Hayward, *Formation and evaporation of nonsingular black holes*, *Phys. Rev. Lett.* **96** (2006) 031103.
- [50] V.P. Frolov, *Notes on nonsingular models of black holes*, *Phys. Rev. D* **94** (2016) 104056.
- [51] E. Ayón-Beato and A. García, *Regular black hole in general relativity coupled to nonlinear electrodynamics*, *Physical Review Letters* **80** (1998) 5056.
- [52] Z.-Y. Fan and X. Wang, *Construction of regular black holes in general relativity*, *Physical Review D* **94** (2016) .
- [53] S.G. Ghosh and R.K. Walia, *Rotating black holes in general relativity coupled to nonlinear electrodynamics*, *Annals of Physics* **434** (2021) 168619.
- [54] S.R. Dolan, M.A.A. de Paula, L.C.S. Leite and L.C.B. Crispino, *Superradiant instability of a charged regular black hole*, *Phys. Rev. D* **109** (2024) 124037.
- [55] M.A.A. de Paula, L.C.S. Leite, S.R. Dolan and L.C.B. Crispino, *Absorption and unbounded superradiance in a static regular black hole spacetime*, *Phys. Rev. D* **109** (2024) 064053.
- [56] H. Yang and Y.-G. Miao, *Superradiance of massive scalar particles around rotating regular black holes**, *Chinese Physics C* **47** (2023) 075101.
- [57] Y. Zhan, H. Xu and S.-J. Zhang, *Charged superradiant instability in a spherical regular black hole*, *Eur. Phys. J. C* **84** (2024) 1315 [[2410.19261](#)].
- [58] Z. Li, *Scalar perturbation around rotating regular black hole: Superradiance instability and quasinormal modes*, *Phys. Rev. D* **107** (2023) 044013.
- [59] E. Franzin, S. Liberati, J. Mazza, R. Dey and S. Chakraborty, *Scalar perturbations around rotating regular black holes and wormholes: Quasinormal modes, ergoregion instability, and superradiance*, *Phys. Rev. D* **105** (2022) 124051.
- [60] E. Franzin, S. Liberati, J. Mazza, A. Simpson and M. Visser, *Charged black-bounce spacetimes*, *Journal of Cosmology and Astroparticle Physics* **2021** (2021) 036.
- [61] Y. Guo and Y.-G. Miao, *Charged black-bounce spacetimes: Photon rings, shadows and observational appearances*, *Nuclear Physics B* **983** (2022) 115938.
- [62] A. Simpson and M. Visser, *Black-bounce to traversable wormhole*, *Journal of Cosmology and Astroparticle Physics* **2019** (2019) 042.
- [63] A. Simpson, P. Martín-Moruno and M. Visser, *Vaidya spacetimes, black-bounces, and traversable wormholes*, *Classical and Quantum Gravity* **36** (2019) 145007.
- [64] F.S. Lobo, A. Simpson and M. Visser, *Dynamic thin-shell black-bounce traversable wormholes*, *Physical Review D* **101** (2020) .
- [65] F.S. Lobo, M.E. Rodrigues, M.V.d.S. Silva, A. Simpson and M. Visser, *Novel black-bounce spacetimes: Wormholes, regularity, energy conditions, and causal structure*, *Physical Review D* **103** (2021) .

- [66] J. Mazza, E. Franzin and S. Liberati, *A novel family of rotating black hole mimickers*, *Journal of Cosmology and Astroparticle Physics* **2021** (2021) 082.
- [67] X. Antoine, E. Lorin and Q.T. and, *A friendly review of absorbing boundary conditions and perfectly matched layers for classical and relativistic quantum waves equations*, *Molecular Physics* **115** (2017) 1861.
- [68] B. Engquist and A. Majda, *Absorbing boundary conditions for numerical simulation of waves*, *Proceedings of the National Academy of Sciences* **74** (1977) 1765.
- [69] D. Appelö and G. Kreiss, *Application of a perfectly matched layer to the nonlinear wave equation*, *Wave Motion* **44** (2007) 531.
- [70] M.S. Morris and K.S. Thorne, *Wormholes in spacetime and their use for interstellar travel: A tool for teaching general relativity*, *American Journal of Physics* **56** (1988) 395.
- [71] M.S. Morris, K.S. Thorne and U. Yurtsever, *Wormholes, time machines, and the weak energy condition*, *Phys. Rev. Lett.* **61** (1988) 1446.
- [72] P. Boonserm, T. Ngampitipan, A. Simpson and M. Visser, *Exponential metric represents a traversable wormhole*, *Phys. Rev. D* **98** (2018) 084048 [1805.03781].
- [73] P. Boonserm, T. Ngampitipan and M. Visser, *Regge-Wheeler equation, linear stability, and greybody factors for dirty black holes*, *Phys. Rev. D* **88** (2013) 041502 [1305.1416].
- [74] R.-Z. Guo, C. Yuan and Q.-G. Huang, *Near-horizon microstructure and superradiant instabilities of black holes*, *Phys. Rev. D* **105** (2022) 064029 [2109.03376].
- [75] Z.-H. Luo and Y.-L. Zhang, *Superradiant instability of area-quantized Kerr black hole with discrete reflectivity*, *Eur. Phys. J. C* **85** (2025) 507 [2404.10742].
- [76] C.-Y. Zhang, Q. Chen, Y. Liu, Y. Tian, B. Wang and H. Zhang, *Nonlinear self-interaction induced black hole bomb*, *Phys. Rev. D* **110** (2024) L041505 [2309.05045].